

ELLIPSOID FITTING WITH THE CAYLEY TRANSFORM

OMAR MELIKECHI¹ AND DAVID B. DUNSON^{1,2}

ABSTRACT. We introduce an algorithm, *Cayley transform ellipsoid fitting* (CTEF), that uses the Cayley transform to fit ellipsoids to noisy data in any dimension. Unlike many ellipsoid fitting methods, CTEF is ellipsoid specific – meaning it always returns elliptic solutions – and can fit arbitrary ellipsoids. It also outperforms other fitting methods when data are not uniformly distributed over the surface of an ellipsoid. Inspired by calls for interpretable and reproducible methods in machine learning, we apply CTEF to dimension reduction, data visualization, and clustering. Since CTEF captures global curvature, it is able to extract nonlinear features in data that other methods fail to identify. This is illustrated in the context of dimension reduction on human cell cycle data, and in the context of clustering on classical toy examples. In the latter case, CTEF outperforms 10 popular clustering algorithms.

1. INTRODUCTION

The problem of fitting ellipsoids to data has applications to statistics, data visualization, feature extraction, pattern recognition, computer vision, medical imaging, and robotics [13, 14]. Existing fitting methods either do not apply in more than 3 dimensions, cannot fit arbitrary ellipsoids, are not *ellipsoid specific* (meaning they may return solutions that are not ellipsoids), are not invariant under translations and rotations of data, and/or do not perform well when data are noisy or not uniformly distributed over the surface of an ellipsoid. In this paper we introduce an ellipsoid fitting method, *Cayley transform ellipsoid fitting* (CTEF), that does all of the above and show via extensive experiments that it often outperforms existing algorithms. In particular, CTEF outperforms other methods when data are noisy or concentrate near a proper subset of an ellipsoid rather than uniformly over it, as is common in practice. One disadvantage of our method is that it is slower than the fastest existing method, but this is likely prohibitive only in real-time applications such as adaptive calibration of 3D sensors [20]. On both real and simulated data CTEF routinely converges in under 5 seconds running Python on a standard 2019 MacBook Air.

Organization of paper. In Section 2 we introduce CTEF and establish its properties. In Section 3 we compare it to other ellipsoid fitting methods on simulated data in multiple settings. In Section 4 we apply CTEF to dimension reduction, data visualization, and clustering. This builds on work in [18] which is limited by a method that only fits ellipsoids whose axes are parallel to the standard coordinate axes in Euclidean space. As noted there, many dimension reduction and clustering algorithms are highly complex and heavily parametrized, yielding results that are difficult to interpret or reproduce. In contrast CTEF

¹DEPARTMENT OF STATISTICAL SCIENCE, DUKE UNIVERSITY, DURHAM, NC

²DEPARTMENT OF MATHEMATICS, DUKE UNIVERSITY, DURHAM, NC

both captures nonlinear structure and admits a clear interpretation. Indeed, letting $\|\cdot\|$ be Euclidean norm, every ellipsoid \mathcal{E} in \mathbb{R}^p satisfies

$$\begin{aligned}\mathcal{E} &= \{x \in \mathbb{R}^p : \|A(a)R(x - c)\|^2 = 1\} \\ &= \{R^T A(a)^{-1}\eta + c : \eta \in S^{p-1}\}\end{aligned}\tag{1.1}$$

for some p -by- p diagonal matrix $A(a)$ with diagonal entries $a_i > 0$, special orthogonal matrix¹ $R \in SO(p)$, and $c \in \mathbb{R}^p$. The reciprocals $1/a_i$ are the lengths of the principal axes of \mathcal{E} , R is a rotation that determines its orientation, and c is its center. Equivalently, \mathcal{E} is obtained from the unit sphere $S^{p-1} = \{\eta \in \mathbb{R}^p : \|\eta\| = 1\}$ by *scaling* the sphere by A^{-1} , *rotating* by R^T , and *translating* by c . CTEF reliably fits A , c , and R , giving a concrete relationship between noisy, nonlinear data and the simple object that is the sphere. The ideas in Section 4 thus stand to contribute to the growing call for interpretable algorithms in machine learning [16, 24]. In Section 5 we elaborate this point and discuss future work.

2. CAYLEY TRANSFORM ELLIPSOID FITTING

In this section we introduce CTEF and prove it is

- (1) ellipsoid specific (Section 2.1).
- (2) able to fit arbitrary ellipsoids (Remark 2.1).
- (3) invariant under rotations and translations of data (Section 2.4).
- (4) convergent (Section 2.5).

CTEF minimizes a loss (Section 2.1) over a *feasible set* (Section 2.2), yielding parameters that define our ellipsoid of best fit; see Equation (2.4). The main idea in what follows is that the Cayley transform, defined below, turns an optimization problem with difficult nonlinear constraints to a problem with simple linear ones, opening the door to a range of optimization algorithms. We use the *STIR* (*Subspace Trust region Interior Reflective*) trust region method introduced in [3] and implemented by the `scipy.optimize.least_squares` package in Python [30]. STIR is specifically designed for bound-constrained nonlinear minimization problems in Euclidean space, making it well-suited to solving objective (2.4). Algorithm 1 outlines CTEF; definitions and details are in the subsections below.

Algorithm 1 Cayley transform ellipsoid fitting (CTEF)

Input: Data $X \in \mathbb{R}^{n \times p}$

1: $Y \leftarrow V^T(X - \bar{x})$

2: $\mathcal{F} \leftarrow \mathcal{F}(Y)$

3: $(a, c, s) \leftarrow \text{STIR}(\mathcal{L}, Y, \mathcal{F})$

▷ Transform data with PCA

▷ Feasible set \mathcal{F} based on Y

▷ Minimize \mathcal{L} over \mathcal{F}

Output: Diagonal matrix $A(a)$, center c , rotation $R(s)$

¹ $SO(p) = \{R \in \mathbb{R}^{p \times p} : R^T R = R R^T = I, \det(R) = 1\}$.

2.1. The loss. Ellipsoids in \mathbb{R}^p are often expressed

$$\mathcal{E} = \{x \in \mathbb{R}^p : (x - c)^T M (x - c) = 1\} \quad (2.1)$$

where M is a symmetric positive definite matrix and c is the ellipsoid center. Eigendecomposing $M = R^T A^2 R$ with A diagonal and $R \in \text{SO}(p)$ shows (2.1) is equivalent to (1.1). The positive definite constraint presents significant difficulty for fitting methods and is why most cannot fit arbitrary ellipsoids or are not ellipsoid specific [13, 27]. To bypass this issue we introduce the *Cayley transform* [5] which maps skew-symmetric matrices S to special orthogonal matrices via $\text{Cay}(S) = (I + S)^{-1}(I - S)$. More specifically, consider fitting an ellipsoid to data $X = \{x^{(i)}\}_{i=1}^n \subseteq \mathbb{R}^p$. To ensure invariance under rotations and translations (Section 2.4) we transform X using *principal component analysis* (PCA) to $Y = \{y^{(i)} = V^T(x^{(i)} - \bar{x})\}$. Here and throughout, $\bar{x} = n^{-1} \sum x_i$ is the mean of X and the *PCA matrix* V is an orthogonal matrix whose columns are eigenvectors² of the covariance matrix of the centered data $\{x^{(i)} - \bar{x}\}$. We always assume eigenvalues are ordered from largest to smallest with columns of V ordered accordingly. So the first column of V corresponds to the largest eigenvalue, the second column to the second largest, and so on. We focus on fitting an ellipsoid to Y ; the best fit ellipsoid for X is then easily obtained by a readily available rotation and translation (Section 2.3).

Having introduced the Cayley transform, we now define our loss. Set $\mathbb{R}_+ = [0, \infty)$. In light of (1.1) it is natural to consider minimizing $L : \mathbb{R}_+^p \times \mathbb{R}^p \times \text{SO}(p) \rightarrow \mathbb{R}_+$ defined by

$$L(a, c, R) = \sum_{i=1}^n (\|A(a)R(y^{(i)} - c)\|^2 - 1)^2, \quad (2.2)$$

but this has constraint $R \in \text{SO}(p)$. Instead, define $\mathcal{L} : \mathbb{R}_+^p \times \mathbb{R}^p \times \mathbb{R}^{p(p-1)/2} \rightarrow \mathbb{R}_+$ by

$$\mathcal{L}(a, c, s) = \sum_{i=1}^n (\|A(a)R(s)(y^{(i)} - c)\|^2 - 1)^2. \quad (2.3)$$

This is identical to (2.2) but now $R : \mathbb{R}^{p(p-1)/2} \rightarrow \text{SO}(p)$ is³ $\text{Cay} \circ S$ where S is the identification of $\mathbb{R}^{p(p-1)/2}$ with the space $\mathfrak{so}(p)$ of skew-symmetric matrices, e.g.

$$S(s_1, s_2, s_3) = \begin{pmatrix} 0 & s_1 & s_2 \\ -s_1 & 0 & s_3 \\ -s_2 & -s_3 & 0 \end{pmatrix}$$

when $p = 3$. The Cayley transform has several well-established and desirable properties. First, it maps skew-symmetric matrices to special orthogonal matrices so any triple (a, c, s) produces an ellipsoid of the form (1.1), proving Claim (1). It is also a surjection onto

$$\text{SO}(p)_* = \{R \in \text{SO}(p) : -1 \text{ is not an eigenvalue of } R\}$$

so minimizing (2.3) can fit every ellipsoid except those in a set of measure zero. This is in stark contrast to existing ellipsoid-specific methods that can only fit ellipsoids with axis

²Also known as *principal components* in PCA terminology.

³Here \circ denotes function composition, i.e. $f \circ g(x) = f(g(x))$.

ratio⁴ at most 2 or axes that are parallel to the standard coordinate axes [13, 18]. While the above proves an almost sure version of Claim (2), the full claim is justified as follows.

Remark 2.1. *It was shown in [12] that every $R \in \text{SO}(p)$ satisfies $R = \text{Cay}(S)D$ for some $S \in \mathfrak{so}(p)$ with entries $|s_{ij}| < 1$ and diagonal matrix D with diagonal entries ± 1 . See also [9]. Thus replacing $\text{Cay}(S)$ with $\text{Cay}(S)D$ in our minimization problem guarantees every ellipsoid can be obtained by such an objective, not just those in $\text{SO}(p)_*$. Moreover, the set $\mathbb{R}^{p(p-1)/2}$ in which the s variables reside could be replaced by $[-1, 1]^{p(p-1)/2}$. We do not pursue this direction however since numerical results suggest no need to include D in practice.*

The next result gives the gradient of \mathcal{L} . This allows us to replace approximate differentiation schemes in gradient-based algorithms like STIR with an exact closed form expression, significantly improving computational performance.

Proposition 2.2. *Fix $x \in \mathbb{R}^p$ and define $\ell : \mathbb{R}_+^p \times \mathbb{R}^p \times \mathbb{R}^{p(p-1)/2} \rightarrow \mathbb{R}$ by $\ell(a, c, s) = \frac{1}{2} \|AR(x - c)\|^2$ with $A = \text{diag}(a)$ and $R = \text{Cay}(S(s))$ as above. Then*

$$\nabla_a \ell(a, c, s) = a^T \text{diag}(y \odot y)$$

$$\nabla_c \ell(a, c, s) = -y^T R^T A^2 R$$

$$\nabla_s \ell(a, c, s) = B^T - B$$

where $y = x - c$, \odot is the Hadamard product, and $B = (I - S(s))^{-1} A^2 R y y^T (I + R^T)$.

Proof. Note $\ell(a, c, s) = \frac{1}{2} y^T R^T A^2 R y$. The expressions for $\nabla_a \ell$ and $\nabla_c \ell$ follow immediately from standard rules of differentiation. The expression for $\nabla_s \ell$ follows from [9, Theorem 3.2] which in our notation states $\nabla_s \ell(s) = B^T - B$ with

$$B = (I - S(s))^{-1} \nabla_R \ell (I + R^T).$$

Again by standard rules of differentiation $\nabla_R \ell = A^2 R y y^T$ and the result follows. \square

The next important example shows \mathcal{L} is globally minimized as certain parameters go to infinity. This motivates our restriction to feasible sets described in the next section.

Example 2.3. *If all data lie exactly on $\mathcal{E} = \{x : \|A(a)R(s)(x - c)\|^2 = 1\}$, then clearly a , c , and s are global minimizers of \mathcal{L} . But \mathcal{L} is also globally minimized as $1/a$ and⁵ c go to infinity. To see why, consider the 2-dimensional example where $1/a = (m, m)$ and $c = (m, 0)$ for $m \in \mathbb{N}$ and $s = 0$ (so $R = I$). Direct computation shows that for any $x \in \mathbb{R}^2$,*

$$\lim_{m \rightarrow \infty} \|AR(x - c)\|^2 = \lim_{m \rightarrow \infty} \frac{(m - x_1)^2 + x_2^2}{m^2} = 1.$$

Hence $\lim_{m \rightarrow \infty} \mathcal{L}(a, c, s) = 0$ whenever the number of data points is finite. Intuitively, \mathcal{L} is minimized by ellipsoids with infinite axis lengths and whose centers are infinitely far from the data.

⁴Throughout this paper, *axis ratio* is the ratio between the largest and smallest axis lengths of an ellipsoid.

⁵For $a \in \mathbb{R}_+^p$ we define $1/a = (1/a_1, \dots, 1/a_p)$.

2.2. The feasible set. To avoid infinite solutions (Example 2.3) and guarantee convergence (Section 2.5) we restrict the domain $\mathbb{R}_+^p \times \mathbb{R}^p \times \mathbb{R}^{p(p-1)/2}$ of \mathcal{L} to a *feasible set* $\mathcal{F} = [a^-, a^+] \times [c^-, c^+] \times [s^-, s^+]$ where $[a^-, a^+]$ is the rectangle $[a_1^-, a_1^+] \times \cdots \times [a_p^-, a_p^+]$ in \mathbb{R}^p and $[c^-, c^+]$ and $[s^-, s^+]$ are defined similarly. Thus axis lengths $1/a_i$ satisfy $1/a_i^+ \leq 1/a_i \leq 1/a_i^-$ and c lies in $[c^-, c^+]$. Empirical studies indicate s^- and s^+ are inconsequential provided $s_i^- \leq -1 < 1 \leq s_i^+$, which is unsurprising given the result of Kahan discussed in Remark 2.1. Our code uses default values $s_i^- = -5$ and $s_i^+ = 5$ for all i . The bound a^+ is also inconsequential provided it is sufficiently large; we set $a_i^+ = 10^{300}$ for all i so no axis can have length smaller than 10^{-300} . To choose a^- , c^- , and c^+ , for $1 \leq j \leq p$ define

$$c_j^- = \min_{1 \leq i \leq n} y_j^{(i)}, \quad c_j^+ = \max_{1 \leq i \leq n} y_j^{(i)}, \quad m_j = c_j^+ - c_j^-.$$

Our default for a^- is $(10 \max_j m_j)^{-1}$ and the default rectangle for c is

$$w[c^-, c^+] = w[c_1^-, c_1^+] \times \cdots \times w[c_p^-, c_p^+]$$

where $w > 0$ determines the size of \mathcal{F} (Figure 1) and is set to a default of $1/2$. The weight w is largely inconsequential when data are relatively uniform over the ellipsoid, but can be significant when data concentrate near a proper subset of the ellipsoid (Figure 2). While we hope to soon automate the choice of w (Section 5.1), for the moment we recommend selecting w based on exploratory analysis of the data at hand.

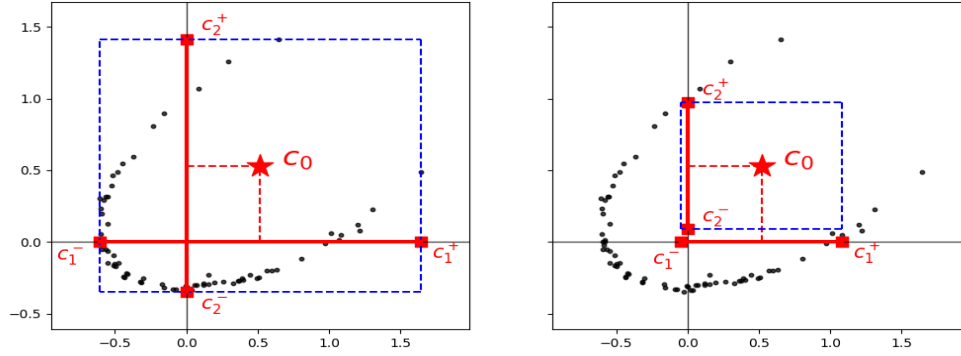


FIGURE 1. Feasible sets (blue) for the center when $w = 1$ (left) and $w = 0.5$ (right). Samples are drawn from the Ellipsoid-Gaussian distribution described in Section 3 with $\tau = 2$ and 1% noise, then transformed with PCA. The star c_0 marks the midpoint of $w[c^-, c^+]$ and is the default initial value in our algorithm. The initial value for a is the vector of all ones. Note c_0 does not depend on w .

2.3. The objective. With \mathcal{L} and \mathcal{F} defined, our objective given data $X = \{x^{(i)}\}_{i=1}^n$ is to find

$$(a_*, c_*, s_*) = \arg \min_{(a, c, s) \in \mathcal{F}} \mathcal{L}(a, c, s). \quad (2.4)$$

The resulting ellipsoid $\mathcal{E}_*(Y) = \{y \in \mathbb{R}^p : \|A(a_*)R(s_*)(y - c_*)\| = 1\}$ is an ellipsoid of best fit for the PCA transformed data $Y = \{V^T(x^{(i)} - \bar{x})\}$. Transforming back to X gives

$$\mathcal{E}_*(X) = \{x : \|A(a_*)R(s_*)V^T(x - (Vc_* + \bar{x}))\|^2 = 1\}$$

which is our best fit for X . This is justified since

$$\begin{aligned} A(\mathbf{a})R(s)(\mathbf{y}^{(i)} - \mathbf{c}) &= A(\mathbf{a})R(s)V^T (\mathbf{x}^{(i)} - (V\mathbf{c} + \bar{\mathbf{x}})) \\ &= A(\mathbf{a})\tilde{R}(s)(\mathbf{x}^{(i)} - \tilde{\mathbf{c}}) \end{aligned}$$

where $\tilde{\mathbf{c}} = V\mathbf{c} + \bar{\mathbf{x}}$ and $\tilde{R}(s) = R(s)V^T$. So $L(\mathbf{a}, \mathbf{c}, R(s)) = L(\mathbf{a}, \tilde{\mathbf{c}}, \tilde{R}(s))$ for all \mathbf{a} , \mathbf{c} , and s , where L is the loss (2.2). In particular, $(\mathbf{a}_*, \mathbf{c}_*, s_*)$ satisfies (2.4) if and only if $(\mathbf{a}_*, \mathbf{c}_*, R(s_*))$ minimizes L over \mathcal{F} if and only if $(\mathbf{a}_*, \tilde{\mathbf{c}}_*, \tilde{R}(s_*))$ minimizes L over the feasible set $\tilde{\mathcal{F}} = \{(\mathbf{a}, \tilde{\mathbf{c}}, s) : (\mathbf{a}, \mathbf{c}, s) \in \mathcal{F}\}$, which is just a rotation and translation of the \mathbf{c} coordinates in \mathcal{F} .

2.4. Invariance. It is desirable for ellipsoid fitting algorithms to be invariant under rotations and translations of data [2, 8, 13]. CTEF satisfies these properties. To see this, consider data $X = \{\mathbf{x}^{(i)}\}$ with PCA-transformation $\{V^T(\mathbf{x}^{(i)} - \bar{\mathbf{x}})\}$. Let $Z = \{\mathbf{z}^{(i)} = Q\mathbf{x}^{(i)} + \tau\}$ be an arbitrary rotation and translation of X , where⁶ $Q \in O(p)$ and $\tau \in \mathbb{R}^p$. Direct computation shows the average of the transformed data is $\bar{\mathbf{z}} = Q\bar{\mathbf{x}} + \tau$ and $W = QV$ is an orthogonal matrix whose columns are eigenvectors of its centered covariance matrix. Therefore

$$\begin{aligned} W^T(\mathbf{z}^{(i)} - \bar{\mathbf{z}}) &= V^T Q^T (Q\mathbf{x}^{(i)} + \tau - Q\bar{\mathbf{x}} - \tau) \\ &= V^T(\mathbf{x}^{(i)} - \bar{\mathbf{x}}). \end{aligned} \tag{2.5}$$

Hence X and Z are identical after being transformed by PCA. Since objective (2.4) depends only on PCA-transformed data, Claim (3) holds.

2.5. Convergence. As discussed at the beginning of this section, we use STIR to solve the ellipsoid fitting objective (2.4). Boundedness of \mathcal{F} guarantees convergence of STIR to a local minimum of the loss function \mathcal{L} . This is because the Cayley transform, and hence \mathcal{L} , is twice continuously differentiable [7]. Since \mathcal{F} is compact it must therefore contain a minimum of \mathcal{L} . Furthermore, for any $\theta_0 = (\mathbf{a}_0, \mathbf{b}_0, s_0) \in \mathcal{F}$ the level set

$$\mathcal{L}(\theta_0) = \{\theta = (\mathbf{a}, \mathbf{b}, s) \in \mathcal{F} : \mathcal{L}(\theta) \leq \mathcal{L}(\theta_0)\}$$

is compact as it is both closed⁷ by continuity of \mathcal{L} and bounded by construction. Convergence of STIR to a local minimum then follows from [3, Theorem 3]. See also [6].

Remark 2.4. A potential concern in light of Example 2.3 is that the local minimum to which CTEF converges will often lie on the boundary of the feasible set \mathcal{F} , potentially resulting in a poor fit. Thankfully, STIR greatly diminishes this possibility by implementing a reflection technique that encourages exploration of the interior of \mathcal{F} [3, 6]. While boundary solutions are still possible, our experience shows they seldom occur in practice, especially for data distributed over substantial portions of the ellipsoid. Moreover, when boundary solutions do occur the fits still tend to be good.

3. EXPERIMENTS

We compare CTEF to four other methods: Calafiore plus alternating direction method of multipliers (CADMM) [14], sum-of-discriminants (SOD) [13], fixed constant (FC) [22],

⁶ $O(p) = \{Q \in \mathbb{R}^{p \times p} : Q^T Q = Q Q^T = I\}$.

⁷If θ_m is a sequence in $\mathcal{L}(\theta_0)$ converging to θ_* , then $\mathcal{L}(\theta_*) = \lim_{m \rightarrow \infty} \mathcal{L}(\theta_m) \leq \mathcal{L}(\theta_0)$ and so $\theta_* \in \mathcal{L}(\theta_0)$.

and Bookstein (BOOK) [2]. Our experiments are similar to those in [13] which compare SOD, FC, and BOOK as well as hyperellipsoid-fit (HES) [13] and Taubin (TAUB) [28]. HES is ellipsoid specific but is omitted because it only applies to ellipsoids with axis ratio at most 2 when $p > 2$. TAUB is omitted because it frequently gives non-elliptic solutions in the presence of even minimal noise. CADMM implements the algorithm introduced by Calafiore in [4] but uses ADMM to reduce its complexity. CADMM and CTEF are ellipsoid specific; SOD, FC, and BOOK are not.

3.1. Data simulation. Data $\{x^{(i)}\}_{i=1}^n$ are simulated from the *Ellipsoid-Gaussian model*

$$x^{(i)} = \Lambda \eta_i + c + \epsilon_i \quad (3.1)$$

where $\Lambda = R^T A^{-1}$ with c , A , and R as in (1.1), $\eta_i \sim \text{vMF}(\mu, \tau)$ are independent random variables drawn from the von Mises-Fisher distribution on S^{p-1} , and $\epsilon_i \sim \mathcal{N}_p(0, \sigma^2 I)$ are independent multivariate normal random variables representing noise. Model (3.1) is introduced and studied in detail in [25]. The parameters of $\text{vMF}(\mu, \tau)$ are the mean $\mu \in S^{p-1}$ and measure of spread $\tau \geq 0$. Increasing τ increases the concentration of the distribution about μ , with $\tau = \infty$ corresponding to a delta measure at μ and $\tau = 0$ to the uniform distribution on S^{p-1} . As before, c is the center of the ellipsoid and Λ determines its shape. In our experiments the entries of c are drawn from $\mathcal{N}(0, 10)$. Λ is chosen to have determinant 1 and so that the resulting ellipsoid has a specified axis ratio, r_{ax} . Other axis lengths are chosen uniformly at random between the smallest and largest. The standard deviation σ is specified as a percentage of the diameter of the longest axis of the ellipsoid. Essentially all of these choices are made to agree with those in [13].

3.2. Measures of performance. Several measures of ellipsoid fitting performance exist in the literature. The two we focus on are *offset error*, e_o , and *shape error*, e_s [13]. Offset error is the norm $\|c - c_*\|$ of the difference between the estimated center, c , and the true center c_* of the ellipsoid from which data are simulated. Shape error is

$$e_s = \frac{\sigma_1(\Lambda^{-1} \Lambda_*)}{\sigma_p(\Lambda^{-1} \Lambda_*)} - 1$$

where Λ and Λ_* are the estimated and true shape matrices and σ_1 and σ_p are the largest and smallest singular values of $\Lambda^{-1} \Lambda_*$, respectively. Another class of performance measures is

$$\ell_{p,q}(\Lambda, c) = \sum_{i=1}^n \left| \|\Lambda^{-1}(x^{(i)} - c)\|^p - 1 \right|^q \quad (3.2)$$

for integers p and q [4, 14]. Observe $\ell_{2,2}$ is precisely (2.3). Unlike offset and shape error, $\ell_{p,q}$ errors do not require knowledge of Λ_* and c_* . However, they can be misleading. This is because of Example 2.3, namely losses of the form (3.2) go to 0 as the ellipsoid center and axis lengths go to infinity. Thus $\ell_{p,q}$ can be arbitrarily small for ellipsoid fits that are arbitrarily bad (Figure 2). For this reason we only consider offset and shape error here.

3.3. Results. We consider the concentration parameter τ , noise parameter σ , and axis ratio r_{ax} which, recall, is the ratio between the longest and shortest axis lengths of an ellipsoid. In each experiment we vary the parameter of interest keeping others fixed. One experiment

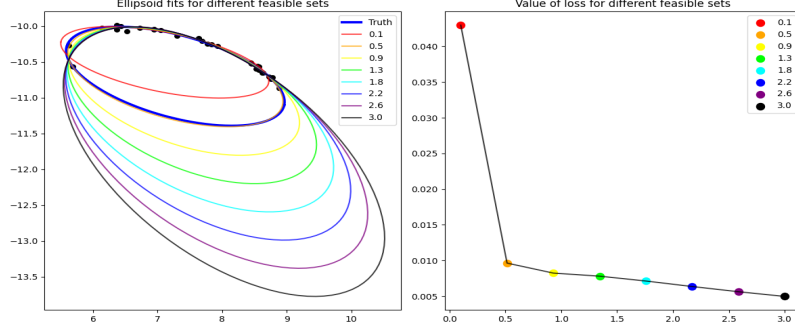


FIGURE 2. (Left) Best fit ellipsoids for different feasible set weights w defined in Section 2.2. Each color represents a different w . The best fit ellipsoid when $w = 0.5$ (orange) closely resembles the true ellipsoid (thick blue curve). (Right) Loss corresponding to each w . For example, the loss when $w = 0.5$ is approximately 0.01. While loss decreases monotonically to 0, centers and axis lengths of the fitted ellipsoids diverge. Here $n = 30$ data points (black dots, left panel) are simulated from the Ellipsoid-Gaussian model with $\tau = 2$ and axis ratio 3.

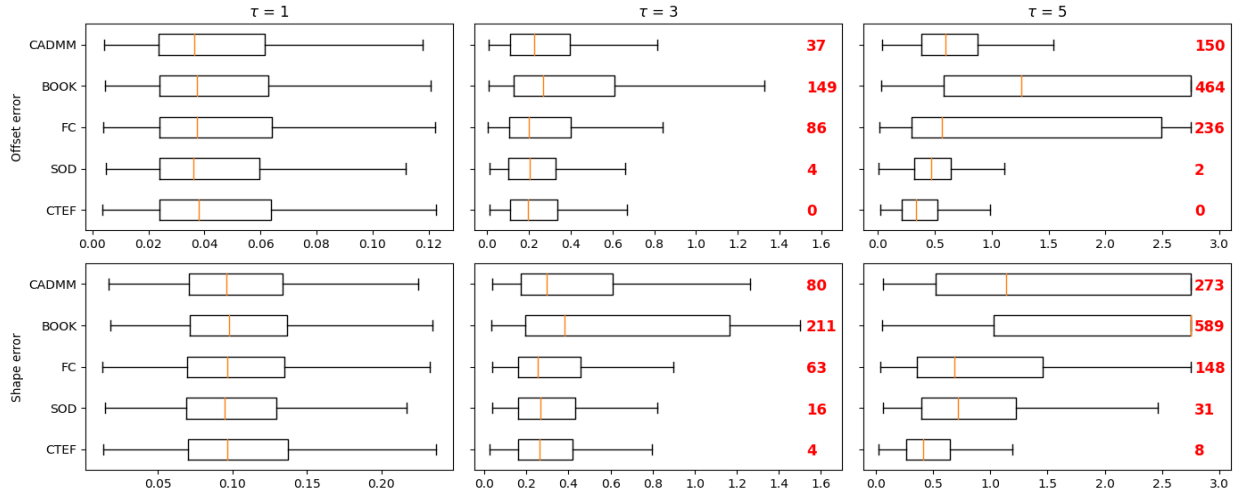


FIGURE 3. Errors for different τ with $p = 3$, $r_{ax} = 2$, noise = 1%, and $n = 18$. Only CTEF remains stable as data become less uniform.

consists of 1000 trials. One trial consists of fitting an ellipsoid to data generated from the Ellipsoid-Gaussian model with the specified parameters using each fitting method. Box plots in Figures 3 to 7 show offset and shape error distributions for each fitting method in each experiment. Medians are indicated by the orange lines and whiskers extend to 1.5 times the interquartile range. Red numbers in some plots indicate the number of times the error for a certain method exceeded a specified threshold, meaning the method either had relatively large error or failed to return an ellipsoid at all. For example, in the upper right panel in Figure 3 the offset error for CADMM exceeds the cutoff in 150 of the 1000 trials.

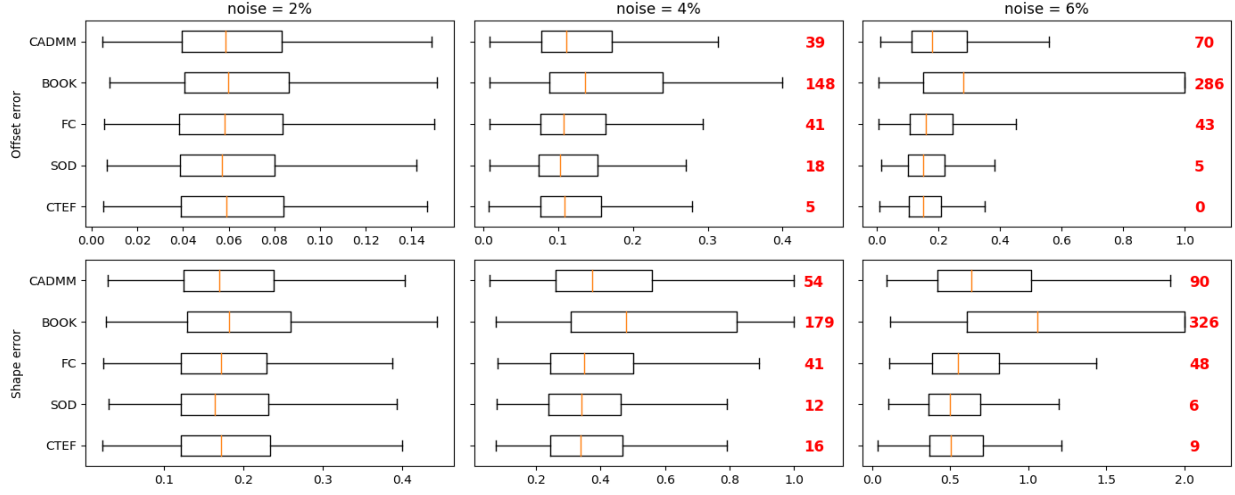


FIGURE 4. Errors for different noise values with $p = 3$, $\tau = 0$, $r_{ax} = 2$, and $n = 18$. Only SOD and CTEF remain stable as noise increases.

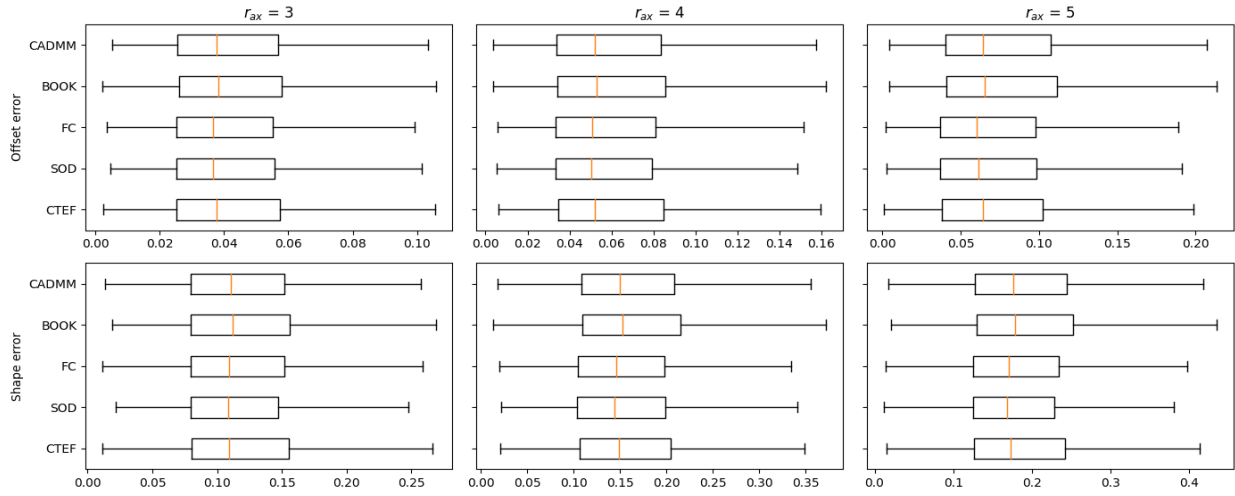


FIGURE 5. Errors for different axis ratios with $p = 3$, $\tau = 0$, noise = 1%, and $n = 18$. In this experiment all methods perform similarly.

Figures 3, 4, and 5 correspond to $p = 3$ and Figures 6 and 7 to $p = 10$. In general, all methods perform similarly when data are uniformly distributed ($\tau = 0$) with low noise. The most pronounced differences occur when data are not uniformly distributed (Figures 3 and 6). CADMM, BOOK, and FC falter when $\tau = 3$ and degenerate significantly when $\tau = 5$, while SOD shows signs of poor performance when $\tau = 5$. Only CTEF remains stable, a finding that is further validated by the Rosenbrock example in Section 4.1 (Figure 9).

The relative robustness of CTEF is due in part to the feasible set which uses the data to confine to “reasonable” ellipsoid parameters and, in particular, prevents solutions from escaping to infinity. In all experiments the axis-length upper bounds $1/\alpha_i^-$ are set to

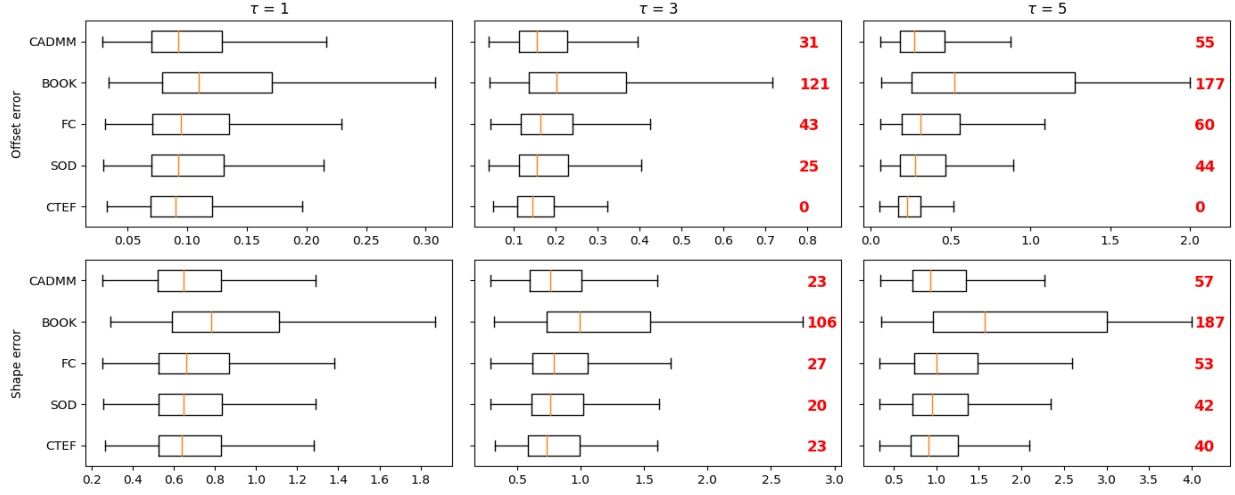


FIGURE 6. Errors for different τ with $p = 10$, $r_{ax} = 2$, noise = 1%, and $n = 80$.

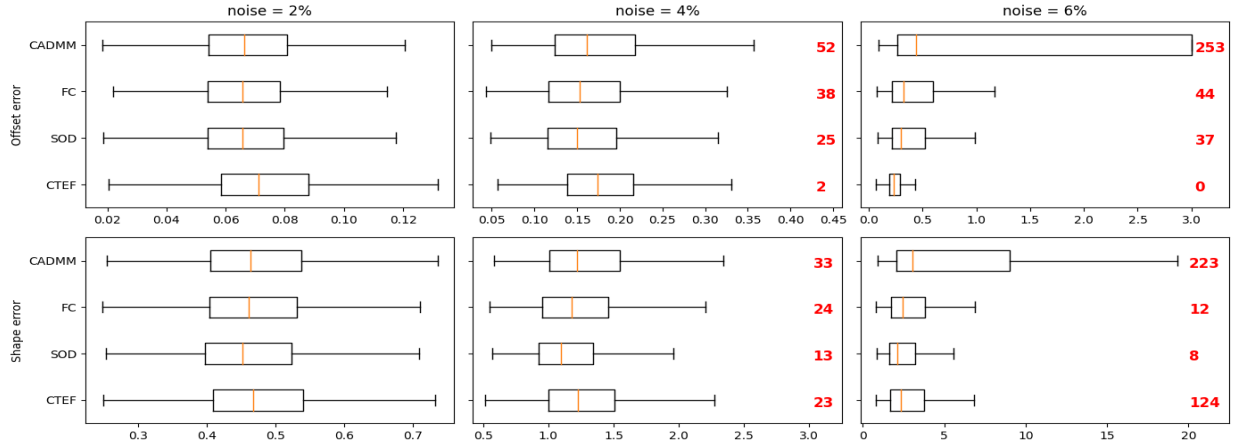


FIGURE 7. Errors for different noise values with $p = 10$, $\tau = 0$, $r_{ax} = 2$, and $n = 150$. BOOK is omitted because it was significantly worse than all other methods.

$1/a_i^- = 10 \max_j m_j$ for all i as discussed above. Thus the only parameter not automatically tuned is the weight w , which is fixed for each parameter value throughout each experiment. For example, in the varying τ experiment in Figure 3, the weights are $w = 0.65$ when $\tau = 1$, $w = 1.2$ when $\tau = 3$, and $w = 2$ when $\tau = 5$. When only one or a handful of datasets are considered as is common in practice, w can be more carefully tuned to obtain better results. Nevertheless, our experiments show that even when w is fixed, CTEF outperforms other methods in the extremely common setting of noisy, non-uniform data, making it the superior method in many practical settings.

So far we have considered fitting p -dimensional ellipsoids to p -dimensional data $X = \{x^{(i)}\}$. For $k < p$ we can instead fit a k -dimensional ellipsoid to X by replacing the p -by- p PCA matrix V with a p -by- k matrix V_k whose k columns are distinct columns of V . The resulting dimension-reduced loss is identical to (2.3) except now $y^{(i)} = V_k^T(x^{(i)} - \bar{x}) \in \mathbb{R}^k$ and the feasible set, which was a $(3 + p)p/2$ dimensional rectangle, is now $(3 + k)k/2$ dimensional. Often V_k will consist of the first k columns of V which, recall, are assumed to be principal components corresponding to the k largest eigenvalues of the covariance matrix of the centered data. However, the Rosenbrock example below shows that using the first k principal components is not always optimal.

In Sections 4.1 and 4.2 we apply our ellipsoid fitting method to nonlinear dimension reduction in two examples: data generated from the hybrid Rosenbrock model [17] and human cell cycle data [26]. In Section 4.3 we present a clustering algorithm based on ellipsoid fitting and show it outperforms 10 other clustering algorithms on several toy examples. All of the examples in this section – especially the human cell cycle example – also illustrate the usefulness of ellipsoid fitting as a data visualization tool.

4.1. Rosenbrock. The Rosenbrock function [21] is often used to test optimization algorithms due to its simple yet numerically challenging geometry. In this example we fit an ellipsoid to data generated from a 3-dimensional hybrid Rosenbrock model [17] with parameters from [25, Section 5.2]. Specifically, 2000 data points $X = \{x^{(i)}\}$ are drawn from the probability density on \mathbb{R}^3 proportional to

$$\rho(x_1, x_2, x_3) \propto \exp(-x_1^2 - 30(x_2 - x_1^2)^2 - (x_3 - x_2^2)^2).$$

Exploratory analyses, namely visualization and PCA, indicate data concentrate near a 2-dimensional ellipse. Our goal therefore is to fit X with a 2-dimensional ellipse using one of $V_2^{(1,2)} = (v_1, v_2)$, $V_2^{(1,3)} = (v_1, v_3)$, or $V_2^{(2,3)} = (v_2, v_3)$ in place of V_k as described above, where v_i is the i th principal component of the centered data. To choose which pair to use, we ran CTEF in each case and picked the (i, j) that minimizes the loss (2.3) with $V_2^{(i,j)}$ in place of V . The left panel in Figure 8 shows $V_2^{(1,3)}$ is best in this regard, a finding that is strongly supported by plotting the corresponding ellipsoids of best fit. In particular, using the leading two principal components, $V_2^{(1,2)}$, is suboptimal. This reflects the fact that, while variance in X is maximized among all 2-dimensional subspaces when data are projected onto the subspace spanned by v_1 and v_2 by definition of PCA, the most pronounced curvature in the PCA transformed data lies in the (v_1, v_3) plane.

4.2. Cell cycle. The *cell cycle* is the process of cell division. It progresses through 4 phases: G_1 (gap 1), S (DNA synthesis), G_2 (gap 2), and M (mitosis). Schematically,

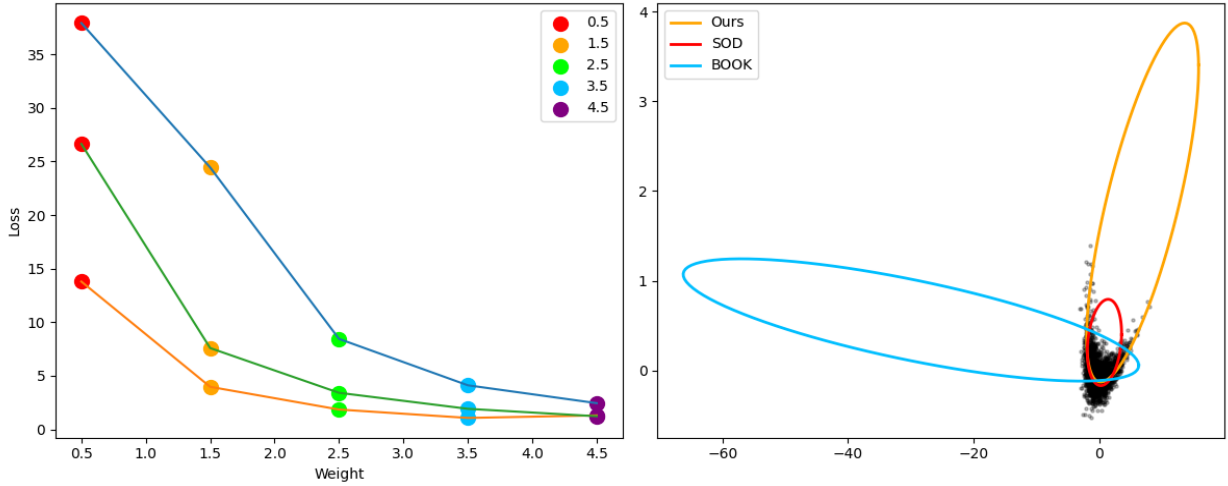


FIGURE 8. (Left) Value of loss (2.3) corresponding to $V_2^{(1,2)}$ (blue line), $V_2^{(1,3)}$ (orange line), and $V_2^{(2,3)}$ (green line), for feasible set weights $w \in \{0.5, 1.5, 2.5, 3.5, 4.5\}$. $V_2^{(1,3)}$ yields the smallest loss for each weight. The “scree” nature of this plot indicates the ellipses corresponding to 1.5 or 2.5 are likely best; see Figure 9. (Right) Black dots are Rosenbrock data X projected onto the subspace spanned by the first and third principal components, v_1 and v_3 . Ellipses are then fit using the methods discussed in this paper. FC is omitted because it returned an ellipse whose largest axis length was magnitudes larger than the ones shown. CADMM is omitted because it failed to return any solution at all. This agrees with our finding in Section 3 that other methods perform poorly when data are not uniformly distributed over an ellipse.

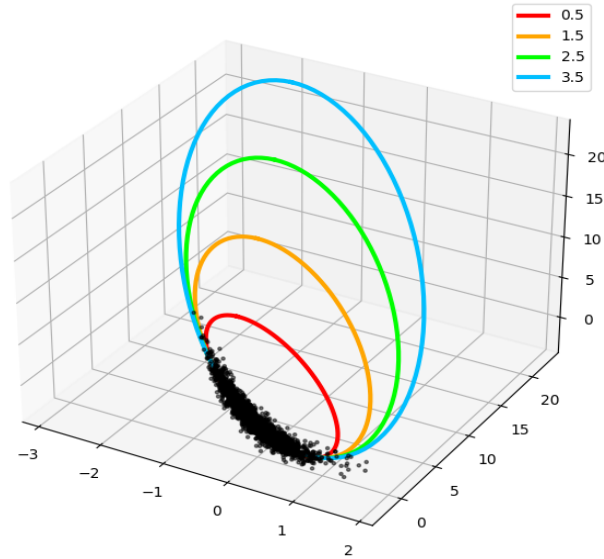
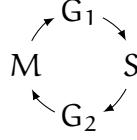


FIGURE 9. Ellipses fit to hybrid Rosenbrock data using CTEF for different weights w .



In [26] the authors identify $p = 40$ core cell cycle features based on studies of $n = 8850$ individual cells. One of their principal goals is visualization. Figure 10 shows two views of their data projected onto the optimal ellipsoid returned by our algorithm. In addition to accurately grouping the 4 cell cycle phases and preserving the cyclic ordering $G_1 \rightarrow S \rightarrow G_2 \rightarrow M \rightarrow G_1$, the fit also captures relative variability of each phase, with G_1 the longest lasting, S and G_2 having similar time frames, and M the most brief [11]. Figure 11 shows 2-dimensional representations of the data using other dimension reduction methods, namely PCA, tSNE [29], UMAP [15], Isomap [1], and locally linear embedding (LLE) [23]. In Section 5 we discuss several of these methods and compare them to ours.

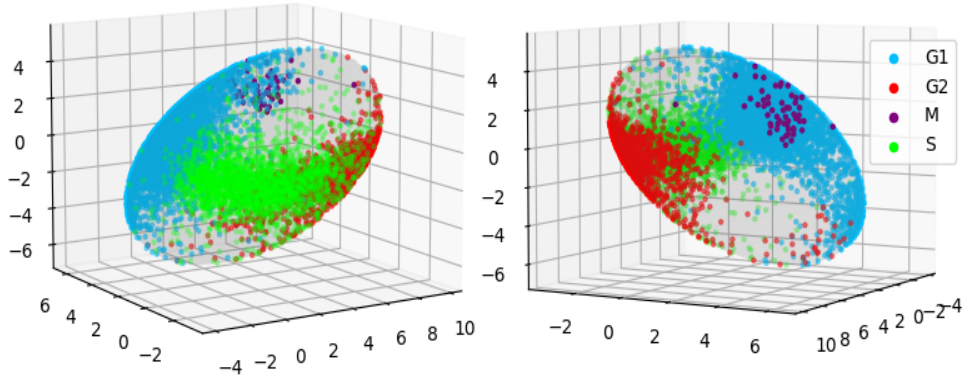


FIGURE 10. Two views of 40-dimensional cell cycle data fitted to an ellipsoid ($n = 8850$).

4.3. Clustering Algorithm 2 gives a clustering algorithm based on our ellipsoid fitting method that is similar to [18, Algorithm 2]. The procedure is simple: Given data $X = \{x^{(i)}\}_{i=1}^n \subseteq \mathbb{R}^p$ with cluster assignments $\kappa = (\kappa_1, \dots, \kappa_n)$ (so $x^{(i)}$ belongs to cluster κ_i), at each step of the algorithm do (1) fit an ellipsoid $\mathcal{E}_j = (A_j, R_j, c_j)$ to data $\{x_i : \kappa_i = j\}$ in the j th cluster, then (2) for each i and each j assign $x^{(i)}$ to the cluster that minimizes the residual error $(\|A_j R_j(x^{(i)} - c_j)\|^2 - 1)^2$. Since the emphasis of this paper is on ellipsoid fitting, we leave detailed analysis of Algorithm 2 to future work. However, preliminary experiments shown in Figures 12, 13, and 14 are promising: Ours is the only algorithm that gives good

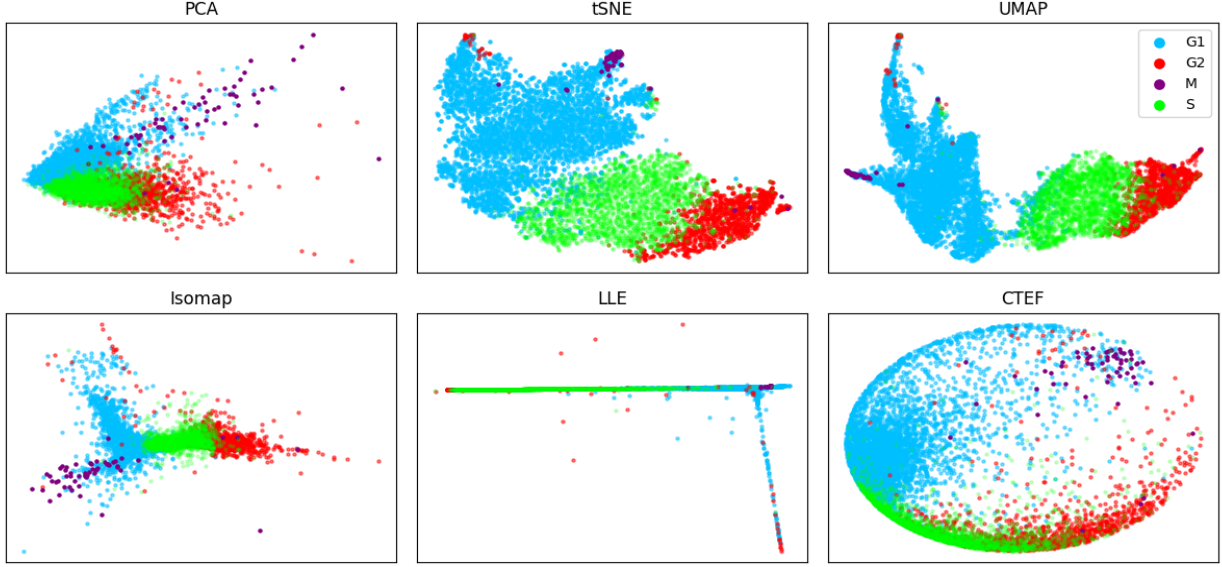


FIGURE 11. *Different dimension reduction techniques applied to 40-dimensional cell cycle data ($n = 8850$).*

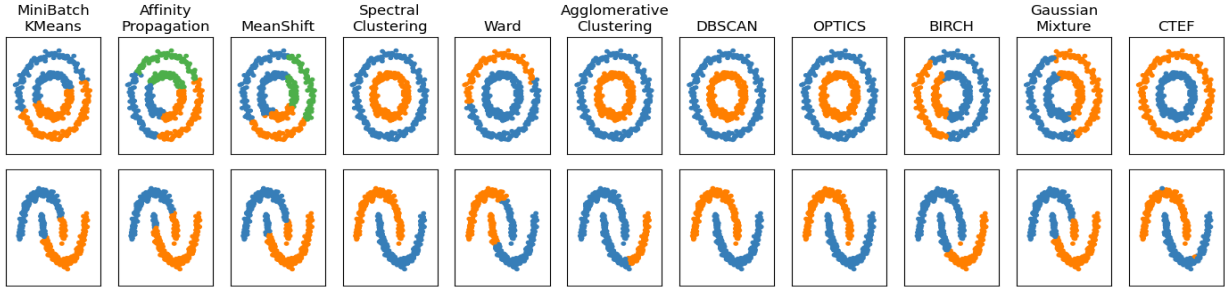


FIGURE 12. *Clustering 500 samples from noisy circles and noisy moons data. Code and results for all algorithms other than ours are reproduced exactly from https://scikit-learn.org/stable/auto_examples/cluster/plot_cluster_comparison.html [19]. They state “parameters of each of these dataset-algorithm pairs has been tuned to produce good clustering results.” Despite this, only spectral clustering, DBSCAN, OPTICS, and CTEF accurately cluster both datasets.*

results in all cases when compared to 10 other clustering algorithms implemented by the popular scikit-learn machine learning Python package [19].

5. DISCUSSION

We have introduced an ellipsoid fitting method that uses the Cayley transform to recast ellipsoid fitting as a bound-constrained minimization problem in Euclidean space. Unlike many existing methods, ours is ellipsoid specific, can fit arbitrary ellipsoids, and is invariant under rotations and translations of data. In addition, the experiments in Section 3 indicate

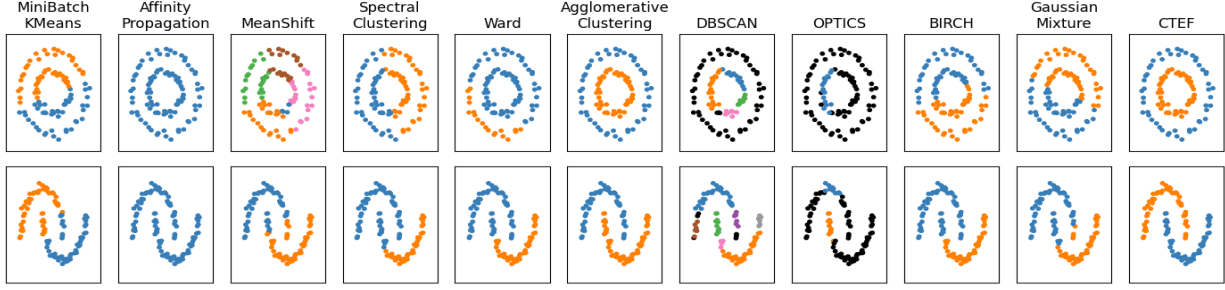


FIGURE 13. Only agglomerative clustering and CTEF accurately cluster when sample size is reduced from 500 samples (Figure 12) to 100.

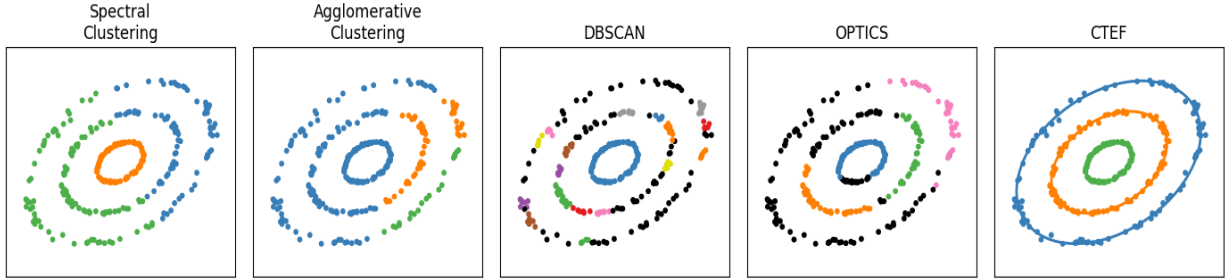


FIGURE 14. Clustering 300 samples from 3 noisy ellipses. Methods that performed poorly in Figures 12 and 13 also performed poorly here and are omitted. Of those shown, ours is the only algorithm that accurately clusters the data. The 3 ellipsoids returned by our algorithm are pictured in the CTEF panel. This illustrates that, in addition to better clustering, CTEF returns a simple, closed-form parametrization of the ellipses corresponding to each cluster.

Algorithm 2 Ellipsoid clustering

Input: Data $X \in \mathbb{R}^{n \times p}$, number of clusters n_c , number of steps n_s

- 1: Initialize clusters $\kappa = (\kappa_1, \dots, \kappa_n) \in \{1, \dots, n_c\}^n$
- 2: $i \leftarrow 0$
- 3: **while** $i < n_s$ **do**
- 4: **for** $0 \leq j < n_c$ **do**
- 5: $\mathcal{E}_j \leftarrow \text{ellipsoid_fit}(\{x_m : \kappa_m = j\})$
- 6: **end for**
- 7: **for** $1 \leq m \leq n$ **do**
- 8: $\kappa_m \leftarrow \arg \min_j (\|A_j R_j (x_m - c_j)\|^2 - 1\|)^2$
- 9: **end for**
- 10: $i \leftarrow i + 1$
- 11: **end while**

Output: Clusters κ , parameters $\{A_j, R_j, c_j\}_{j=1}^{n_c}$

CTEF outperforms others when data concentrate near a proper subset of an ellipsoid, a finding that is further highlighted by the Rosenbrock example in Section 4.1 (Figure 9).

In Section 4 we saw examples of how CTEF – and ellipsoid fitting in general – can be used for dimension reduction and clustering. In all examples the only parameter to tune was the weight w that determines the size of the rectangle in which the fitted ellipsoid center must lie (Figure 1). This stands in stark contrast to many popular dimension reduction (DR) and clustering algorithms that require careful tuning of parameters. As stated recently in [10], *“DR methods often become widely used without being carefully evaluated, and these methods may contain flaws that are unknown to their users. As further evidence of this, there are now many papers explaining how to use various popular DR methods effectively...These papers are only necessary because DR results are often misleading, and because DR cannot be trusted out-of-the box. These papers, which teach us how to manipulate parameters of DR algorithms, highlight the urgent need to develop trustworthy DR methods.”* The authors go on to demonstrate tSNE and UMAP can be highly sensitive to parameter choices, can behave differently under different random seeds (making results difficult to reproduce), and can fail to capture global structure in data. Since CTEF is deterministic it is entirely reproducible; once the feasible set and initial condition are specified, it always returns the same result. Furthermore, as the cell cycle example shows, ellipsoid fitting methods can capture global curvature and/or cyclic patterns in data. This is further evidenced by the success of ellipsoid clustering relative to other methods in Section 4.3. Like dimension reduction, many clustering algorithms are sensitive to potentially unintuitive parameter choices and can fail to capture global structure due to dependence on local parameter specifications such as number of nearest neighbors. For example, it is particularly clear in Figure 14 that all methods besides ours only capture local curvature, failing to distinguish the three globally distinct ellipses that are abundantly clear to the naked eye.

5.1. Future work We see two primary directions for future work. In terms of the fitting algorithm itself, there is likely room for improvement in computational efficiency. In [13] the authors suggest combining direct methods such as SOD, FC, and BOOK with iterative methods such as CADMM and now CTEF. Since direct methods are faster, this could reduce the time complexity. It would also be useful to have a more principled method for choosing the feasible set, specifically the weight w , which can play an important role when data look like the Rosenbrock data or the data in Figure 2. One approach implemented in our work is to compute the minimal loss \mathcal{L} for distinct values of w and choose the w at the “elbow” of the plot, e.g. $w = 0.5$ in Figure 2 or $w = 1.5$ in Figure 8. However, choosing initial weights and identifying the elbow is subjective. An alternative method we are currently pursuing is to train a function using data generated from the Ellipsoid-Gaussian model to automatically choose w .

The other main line of future work is to extend the results of Section 4. While we make no claim that ellipsoid fitting is a silver bullet – surely there are data on which it would perform poorly – our examples indicate it is a promising tool for capturing nonlinearities and global features in data that are missed by many popular dimension reduction and clustering algorithms. As an immediate next step it is interesting to test CTEF on data that are known or suspected to be curved or cyclic in nature. In the context of dimension reduction, one could replace our initial PCA step with a different dimension reduction technique before ellipsoid fitting. Similarly, we initiate our clustering algorithm with

k-means. An obvious modification is to initiate with a different clustering algorithm to improve performance. Finally, it is good to establish further theory for ellipsoid fitting as a dimension reduction and clustering technique, both to obtain rigorous guarantees to shed light on practical limitations and viable enhancements.

Code availability. Code for this work is available at <https://github.com/omelikechi/ctef>.

ACKNOWLEDGMENTS

The authors thank Andrea Agazzi, Didong Li, Katerina Papagiannouli, and Hanyu Song for helpful conversations. We also thank the authors of [13, 14] for providing and answering questions about their code. This project has received funding from the European Research Council (ERC) under the European Union’s Horizon 2020 research and innovation programme (grant agreement No 856506). It is also supported by National Institutes of Health grants R01-ES027498 and R01-ES028804 and Office of Naval Research grant 00014-21-1-2510-P00001. OM also thanks NSF-DMS-2038056 for partial support.

REFERENCES

- [1] M. Balasubramanian and E. L. Schwartz. The isomap algorithm and topological stability. *Science*, 295(5552):7–7, 2002.
- [2] F. L. Bookstein. Fitting conic sections to scattered data. *Computer Graphics and Image Processing*, 9(1):56–71, 1979.
- [3] M. A. Branch, T. F. Coleman, and Y. Li. A subspace, interior, and conjugate gradient method for large-scale bound-constrained minimization problems. *SIAM J. Sci. Comput.*, 21:1–23, 1999.
- [4] G. Calafiore. Approximation of n-dimensional data using spherical and ellipsoidal primitives. *IEEE Transactions on Systems, Man, and Cybernetics - Part A: Systems and Humans*, 32(2):269–278, 2002.
- [5] A. Cayley. On the theory of the analytical forms called trees. *The London, Edinburgh, and Dublin Philosophical Magazine and Journal of Science*, 13(85):172–176, 1857.
- [6] T. F. Coleman and Y. Li. An interior trust region approach for nonlinear minimization subject to bounds. *SIAM Journal on Optimization*, 6(2):418–445, 1996.
- [7] E. Faou, E. Hairer, M. Hochbruck, and C. Lubich. Geometric numerical integration. *Oberwolfach Reports*, 2022.
- [8] A. Fitzgibbon, M. Pilu, and R. Fisher. Direct least square fitting of ellipses. *IEEE Transactions on Pattern Analysis and Machine Intelligence*, 21(5):476–480, 1999.
- [9] K. Helfrich, D. Willmott, and Q. Ye. Orthogonal recurrent neural networks with scaled Cayley transform. In *International Conference on Machine Learning*, pages 1969–1978. PMLR, 2018.
- [10] H. Huang, Y. Wang, C. Rudin, and E. P. Browne. Towards a comprehensive evaluation of dimension reduction methods for transcriptomic data visualization. *Communications Biology*, 5(1):719, 2022.
- [11] E. Israels and L. Israels. The cell cycle. *The Oncologist*, 5(6):510–513, 2000.
- [12] W. Kahan. Is there a small skew cayley transform with zero diagonal? *Linear Algebra and its Applications*, 417:335–341, 09 2006.
- [13] M. Kesäniemi and K. Virtanen. Direct least square fitting of hyperellipsoids. *IEEE Transactions on Pattern Analysis and Machine Intelligence*, 40(1):63–76, 2018.
- [14] Z. Lin and Y. Huang. Fast multidimensional ellipsoid-specific fitting by alternating direction method of multipliers. *IEEE Transactions on Pattern Analysis and Machine Intelligence*, 38(5):1021–1026, 2016.
- [15] L. McInnes, J. Healy, and J. Melville. Umap: Uniform manifold approximation and projection for dimension reduction. *arXiv preprint arXiv:1802.03426*, 2018.
- [16] C. Molnar. *Interpretable machine learning*. Lulu.com, 2020.

- [17] F. Pagani, M. Wiegand, and S. Nadarajah. An n-dimensional Rosenbrock distribution for Markov chain Monte Carlo testing. *Scandinavian Journal of Statistics*, 49(2):657–680, 2022.
- [18] D. Paul, S. Chakraborty, D. Li, and D. Dunson. Principal ellipsoid analysis (PEA): Efficient non-linear dimension reduction & clustering. *arXiv preprint arXiv:2008.07110*, 2020.
- [19] F. Pedregosa et al. Scikit-learn: Machine learning in Python. *Journal of Machine Learning Research*, 12:2825–2830, 2011.
- [20] T. Pylvänäinen. Automatic and adaptive calibration of 3D field sensors. *Applied Mathematical Modelling*, 32(4):575–587, 2008.
- [21] H. Rosenbrock. An automatic method for finding the greatest or least value of a function. *The Computer Journal*, 3(3):175–184, 1960.
- [22] P. L. Rosin. A note on the least squares fitting of ellipses. *Pattern Recognition Letters*, 14(10):799–808, 1993.
- [23] S. T. Roweis and L. K. Saul. Nonlinear dimensionality reduction by locally linear embedding. *Science*, 290(5500):2323–2326, 2000.
- [24] C. Rudin. Stop explaining black box machine learning models for high stakes decisions and use interpretable models instead. *Nature Machine Intelligence*, 1(5):206–215, 2019.
- [25] H. Song and D. B. Dunson. Curved factor analysis with the Ellipsoid-Gaussian distribution. *arXiv preprint arXiv:2201.08502*, 2022.
- [26] W. Stallaert, K. M. Kedziora, C. D. Taylor, T. M. Zikry, J. S. Ranek, H. K. Sobon, S. R. Taylor, C. L. Young, J. G. Cook, and J. E. Purvis. The structure of the human cell cycle. *Cell systems*, 13(3):230–240, 2022.
- [27] Z. L. Szpak, W. Chojnacki, and A. Van Den Hengel. Guaranteed ellipse fitting with the sampson distance. In *Computer Vision–ECCV 2012: 12th European Conference on Computer Vision, Florence, Italy, October 7–13, 2012, Proceedings, Part V 12*, pages 87–100. Springer, 2012.
- [28] G. Taubin. Estimation of planar curves, surfaces, and nonplanar space curves defined by implicit equations with applications to edge and range image segmentation. *IEEE Transactions on Pattern Analysis and Machine Intelligence*, 13(11):1115–1138, 1991.
- [29] L. Van der Maaten and G. Hinton. Visualizing data using t-SNE. *Journal of Machine Learning Research*, 9(11), 2008.
- [30] P. Virtanen et al. SciPy 1.0: Fundamental algorithms for scientific computing in Python. *Nature Methods*, 17:261–272, 2020.